Relationship between Changes in Crystalline Lens Shape and Axial Elongation in Young Children

Kotaro Ishii,[1] *Masahiro Yamanari,*[2] *Hiroyoshi Iwata,*[3] *Yoshiaki Yasuno,*[2] *and Tetsuro Oshika*[1]

Purpose. To evaluate the relationship between changes in crystalline lens shape and axial elongation during growth in young children.

Methods. Twenty-five patients (age: 1 month to 6 years) who underwent head magnetic resonance imaging (MRI) were included in the analysis. Refractive error was measured with an autorefractor in 22 patients. Crystalline lens dimensions and axial length (AL) were obtained from the MR images. The radius of curvature and asphericity of the crystalline lens were measured using reconstructed MR images. Crystalline lens shape and eyeball shape were numerically expressed by elliptic Fourier descriptors (EFDs) on the basis of MR images. The contours of the crystalline lens and eyeball were evaluated by principal component analysis of the EFDs.

Results. The average anterior and posterior radii of curvature were 6.21 mm (range across ages from 3.89–7.26 mm) and –4.81 mm (range across ages from –2.93 to –5.67 mm). These were closely correlated with age by logarithmic analysis. The first principal component (PC1) of the crystalline lens explained 89.15% of the total variance in lens shape, and it was also significantly correlated with age (Pearson's $r = 0.648$, $P < 0.001$) and AL ($r = 0.847$, $P < 0.001$). In the multiple linear regression analysis in which AL was a dependent variable, only the PC1 of the crystalline lens was associated with AL.

Conclusions. Axial elongation is related to the entire contour of the crystalline lens. This result shows that axial elongation progresses in parallel to change in the crystalline lens shape. (*Invest Ophthalmol Vis Sci.* 2013;54:771–777) DOI:10.1167/iovs.12-10105

The optical development process in which a clear retinal image is obtained by coordination of the dioptric power of the cornea and the crystalline lens and extension of the focal length is known as emmetropization. Many animal studies have been conducted for determining the aspects of the retinal image that might affect the regulation of eye growth.[1–6] We know that the growth of the eye is guided by visual feedback, with the eventual aim being optimal focus of the retinal image or emmetropization.[7,8] Wallman et al.[7] showed that local eye growth is guided by the local refractive error in chicks. However, one research group found no correlation between defocus and changes in refractive error and suggested that these results do not support a simple model of emmetropization in response to the level of hyperopic defocus in human eyes.[9] Therefore, it has been suggested that axial elongation is not determined simply by the refraction value during the emmetropization period.[7–9]

The cornea, which averages 48 diopters (D) of power at birth, loses about 4 D by the age of 2 years.[10,11] The crystalline lens, which averages 45 D of power during infancy, loses about 20 D by the age of 6 years.[12,13] On the other hand, the axial length increases by 5–6 mm over that same time frame.[14] In addition, the balance between corneal and lenticular refractive power and the length of the eye maintains an almost stable refraction state during emmetropization.

A recent longitudinal study of children 6 to 14 years of age reported that normal development of the crystalline lens is characterized by thinning, flattening, and a decrease in power to maintain emmetropia.[15] According to previous reports, axial length (AL) is increased by 3 mm between the ages of 9 months and 9 years, and corneal dioptric power does not change over this period.[16] However, during the same period, because the crystalline lens power has decreased by more than 15.0 D, the change in the focal length is offset by a change in the power of the crystalline lens.[16,17] Therefore, the relationship between changes in crystalline lens and axial elongation is considered essential for emmetropization.[15–17] Sorsby et al.[18] reported values of crystalline lens dimensions and other optical elements in twins in 1962. From these values, van Alphen[19] analyzed a correlation matrix using the data of subjects 4 to 70 years of age, and demonstrated that the anterior and posterior lens surface refractive power significantly correlated with AL. However, few reports have investigated the relationship between changes in crystalline lens shape and eyeball growth in young children.

Numerous previous studies have measured in vivo crystalline lens dimensions in humans using slit-lamp photography,[20] slit-lamp Scheimpflug photography,[20–22] ultrasonography,[23–25] and magnetic resonance imaging (MRI).[26,27] Because it is difficult to obtain an exact slit-lamp image or to perform ultrasonography in infants, we retrospectively evaluated the MR images of the eyeballs of young children using a 3-dimensional (3D) reconstruction technique. The method used for evaluating shape is the main problem associated with comparing crystalline lens shape and AL or eyeball shape because it is difficult to prepare a reference point for comparing two contours that change simultaneously. The importance of this problem has not been considered in previous analyses of eyeball shape. In our previous study, eyeball shape in young children was quantitatively evaluated using a new method of mathematically expressing shape via elliptic Fourier descriptors (EFDs).[28] EFDs, initially proposed

From the [1]Department of Ophthalmology, Faculty of Medicine, University of Tsukuba, Ibaraki, Japan; the [2]Computational Optics Group in the University of Tsukuba, University of Tsukuba, Ibaraki, Japan; and the [3]Laboratory of Biometry and Bioinformatics, Department of Agricultural and Environmental Biology, Graduate School of Agricultural and Life Sciences, the University of Tokyo, Tokyo, Japan.

Submitted for publication April 30, 2012; revised June 25, October 17, November 14, November 21, and December 25, 2012; accepted January 3, 2013.

Disclosure: **K. Ishii**, None; **M. Yamanari**, None; **H. Iwata**, None; **Y. Yasuno**, None; **T. Oshika**, None

Corresponding author: Kotaro Ishii, Department of Ophthalmology, Faculty of Medicine, University of Tsukuba, 1-1-1 Tennoudai, Tsukuba, Ibaraki 305-8575, Japan; ishii_k@md.tsukuba.ac.jp.

by Kuhl and Giardina[29] in 1982, can numerically express any shape with a closed 2-dimensional (2D) contour. Here, we evaluated the relationship between changes in crystalline lens shape and axial elongation in young children by elliptical Fourier analysis on the basis of MR images.

Materials and Methods

Informed consent was obtained from the parent(s)/guardian(s) of all participating patients, and the study was approved by the hospital's ethics committee. We adhered to the stipulations of the Declaration of Helsinki. We used eyeball images taken by MRI to perform quantitative analysis of crystalline lens shape and eyeball shape. Fifty-seven patients (age range: 1 month–6 years) were enrolled in this study. They were examined using head MR images between January and December 2009 at Tsukuba University Hospital. All the patients underwent an ophthalmological examination. None had any history of ocular diseases, trauma, or ophthalmic surgery. No significant findings were observed during slit-lamp microscopy and fundoscopy. The main reasons for undergoing MRI included strabismus, a low Apgar score, headache, and gait disorder. The exclusion criteria for analysis were esotropia, hyperopia over 6 D, intracranial space-occupying lesions, congenital abnormalities, and chromosomal abnormalities. Patients with intermittent exotropia of less than 15 prism diopters were included. Seventeen patients were excluded by esotropia, and exotropia more than 15 prism diopters. Three patients were excluded by intracranial space-occupying lesions. Twelve patients were excluded by congenital and chromosomal abnormalities. Thus, 25 patients were included in the analysis. Of these, 22 patients had their refractive error measured with an autorefractor (Righton Retinomax 2 Autorefractor, Techni Eye, Inc., Tarpon Springs, FL); cycloplegia was induced using 0.5% atropine sulfate during refraction but was not used during the MRI.

MRI

MR images were obtained using a 1.5-Tesla superconducting magnet (Gyroscan Intera and Gyroscan Powertrak 1000; Phillips, Best, The Netherlands) with a phased-array head coil. To obtain a sharply defined contour of the eyeball, we took images of samples using T2-weighted horizontal MR images. T2-weighted images were obtained by the fast spin-echo method (pixel bandwidth, 100–150 kHz; repetition time, 2.5–3 seconds; echo time, 90–130 ms; section thickness, 1.2–2.4 mm; field of view, 70 × 70–95 × 95 mm; flip angle, 90°; and acquisition matrix, 256 × 256–320 × 320).

All patients were sedated using triclofos sodium syrup, and scans were performed with the subject in the supine position. Ocular dimensions were measured using the horizontal images at approximately ×16 magnification on a computer monitor (standard resolution, 512 × 512 pixels). Anterior chamber depth (ACD) and crystalline lens thickness were measured using linear calipers by an author (KI), and the distance between any two points was converted from pixels to millimeters. AL was recorded as the distance between the posterior cornea and the approximate location of the fovea along a line that bisected the eye in the horizontal plane.

This was a retrospective study, and because the MR images were acquired from sedated patients, it was not possible to fix the visual axis on the image. Therefore, a technique that utilized 3D-MR images of the eyeball was used to obtain horizontal MRI sections of the eyeball at an equal height for all analyses (Fig. 1). We used 12–20 unprocessed slices from the horizontal MR images to create the 3D-MR images of the eyeball; 1.2 to 2.4-mm slices were used. Using this procedure, the crystalline lens and the entire eyeball were reconstructed. In contrast, it was difficult to accurately reconstruct the iris at this resolution because it was mostly in the form of lines in a 2D image. This technique has been validated previously.[17] The T2-weighted horizontal MR images that were used for the 3D-reconstruction technique were used to estimate the eyeball geometry.

Digitization of MR Images

In all cases, images of the right eye were used for image processing and contour recording. EFDs can numerically express any shape with a closed 2D contour.[18] The formulation consists of a pair of equations (x and y) derived as functions of a third variable (t). The general equations for EFDs are

$$x(t) = A_0 + \sum_{n=1}^{N}\left(a_n\frac{\cos 2n\pi t}{T} + b_n\frac{\sin 2n\pi t}{T}\right)$$

$$y(t) = C_0 + \sum_{n=1}^{N}\left(c_n\frac{\cos 2n\pi t}{T} + d_n\frac{\sin 2n\pi t}{T}\right)$$

where n equals the harmonic number, N equals the maximum harmonic number, and T equals the length of the contour period. Solutions for the A_0, C_0, a_n, b_n, c_n, and d_n coefficients are required. The EFD coefficients for the crystalline lens and eyeball were calculated by discrete Fourier transformation of the contours of the objects from digital images (Fig. 2A). The EFD coefficients were subsequently standardized to be invariant with respect to size, rotation, and starting point; the procedure was based on the ellipse of the first harmonic. For standardization, the corneal apex and the temporal and nasal sides of the right eye were placed on the right, top, and at the bottom, respectively (Figs. 2B, 2C).

With regard to the harmonic number n, the descriptive power of the shape improves as the maximum value N increases. In this analysis, the N value was set at 20. When $N = 20$, the standardized EFDs comprised 80 standardized Fourier coefficients. Information on shape was maintained in the EFD coefficients. Therefore, progression of the EFD coefficients could be used for various mathematical shape analyses.

Crystalline Lens Image Analysis

The dimensions of the crystalline lens were evaluated on the xy plane of the reconstructed image. The equatorial lens diameter (D), lens thickness (T), anterior lens thickness (Ta), and posterior lens thickness (Tp) are shown in Figure 2C. In this examination, the best-fit ellipse was calculated using the Levenberg–Marquardt algorithm for the anterior and posterior surface of the crystalline lens within the central 120° zone, and the radius of curvature (R) and asphericity (Q) were calculated. The asphericity of ocular surfaces is typically described by surfaces with profiles that are conic sections.[30,31]

In mathematics, a conic section is a curve obtained by intersecting a cone with a plane. The general equations of the best-fit ellipse and the conic curve are

$$\frac{x^2}{r_x^2} + \frac{y^2}{r_y^2} = 1, Q = \frac{r_x^2}{r_y^2} - 1$$

where r_x and Q are the apical radius and asphericity, respectively. The apical direction is along the x-axis. Conic curves are classified as spheres ($Q = 0$, $r_x = r_y$), oblate ellipses ($Q > 0$), or prolate ellipses ($-1 < Q < 0$).

The root mean square (RMS) error was calculated between the data points of the reconstructed eyeball and the fitted ellipsoid. The RMS error provided a goodness-of-fit measure for each ellipsoid calculation.

Principal Component Analysis of EFDs

Because the number of standardized Fourier coefficients was large (i.e., 80 coefficients), it was difficult to analyze the variation of each coefficient and to interpret the analysis results. To summarize the information contained in EFDs, we subjected the EFDs to principal

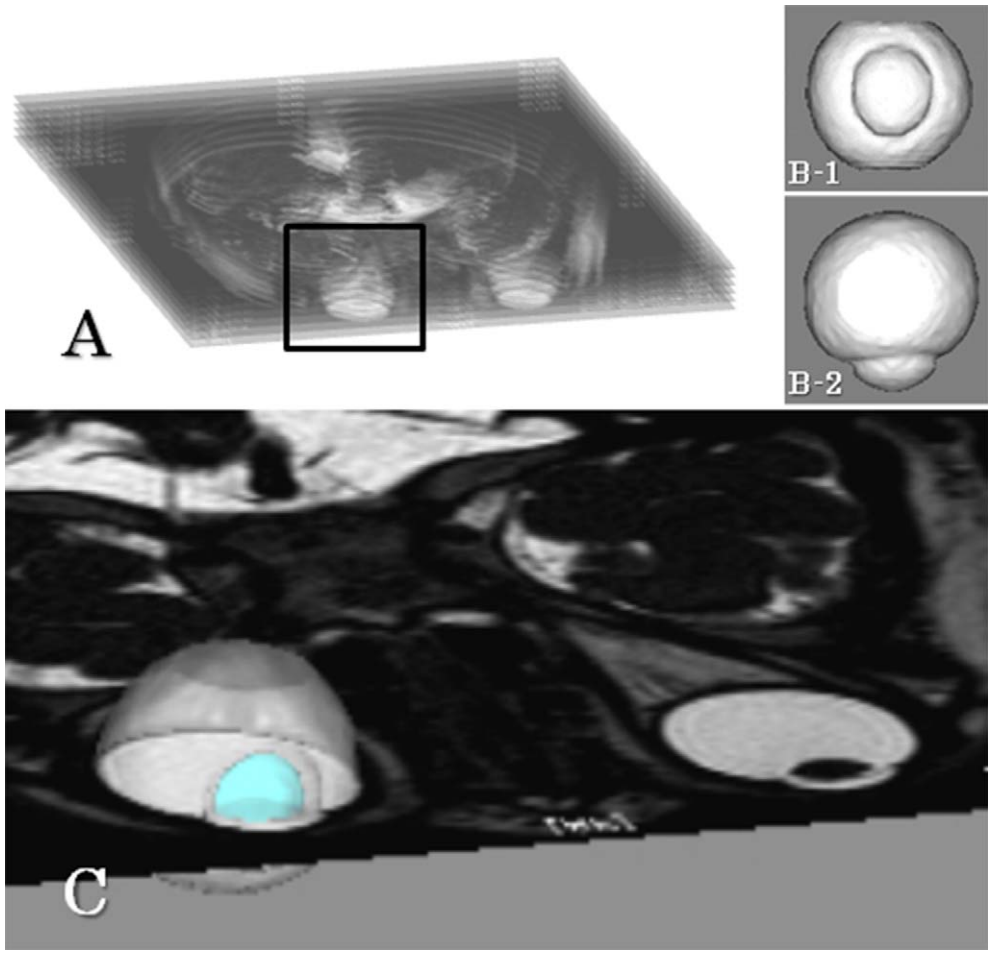

Figure 1. (**A**) Unprocessed horizontal MR image consisting of approximately 12–20 slices used to construct the 3D-MR images of the eyeball. (**B**) Viewpoint from two orthogonal directions of the 3D-MR images of the eyeball. (**C**) The 3D-MR image of the eyeball was used to obtain horizontal MRI sections of the eyeball of each case at an equal height. The object colored *light blue* is the reconstructed crystalline lens.

component analysis (PCA), which is a multivariate analysis technique that decreases the dimension of the original data to facilitate further analysis. PCA was performed on the basis of the variance–covariance matrix of the coefficients as

$$\begin{bmatrix} s_1 \\ s_2 \\ \bullet \\ s_n \end{bmatrix} = \begin{bmatrix} v_{00} & v_{01} & \cdots & v_{0m} \\ v_{10} & \bullet & \cdots & \bullet \\ \bullet & \bullet & \cdots & \bullet \\ v_{m0} & \bullet & \cdots & v_{mm} \end{bmatrix} \begin{bmatrix} a_1^* \\ b_2^* \\ \bullet \\ d_n^* \end{bmatrix}$$

where s_n is the principal component, v_m is the eigenvector, and (a_n^*, b_n^*, c_n^*, d_n^*, . . .) are standardized EFDs. We performed PCA of the EFDs for the crystalline lens and eyeball contours.

This method evaluated the contour obtained from the MR image of the eyeball using several first principal components (s_1, s_2, s_3, . . .). An advantage of PCA of EFDs is that it is possible to reconstruct the contour in reverse from the coefficient values. Utilizing this feature, it is possible to visually describe the characteristics of the shape extracted as principal components.[28,32] This feature makes it easier to interpret the implications of each principal component, which is generally difficult in other analyses.

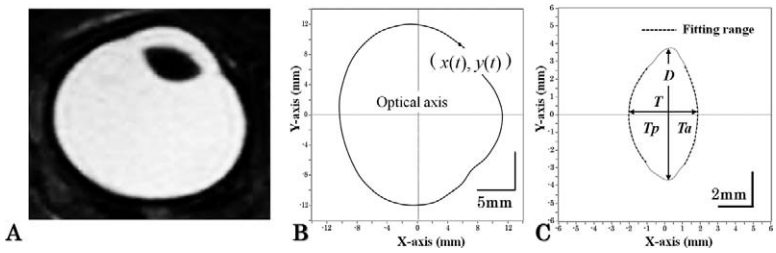

Figure 2. (**A**) The reconstructed T2-weighted horizontal MR image obtained from the right eye was used for image processing and contour recording. (**B**) The *x* and *y* coordinates of the contour of eyeball shape were delineated as periodic functions of distance (*t*) with a period of T. (**C**) *D*, *T*, *Ta*, and *Tp* are shown. The best-fit ellipse was calculated for the anterior and posterior surface within the central 120° zone. *R* and *Q* were calculated within the zone.

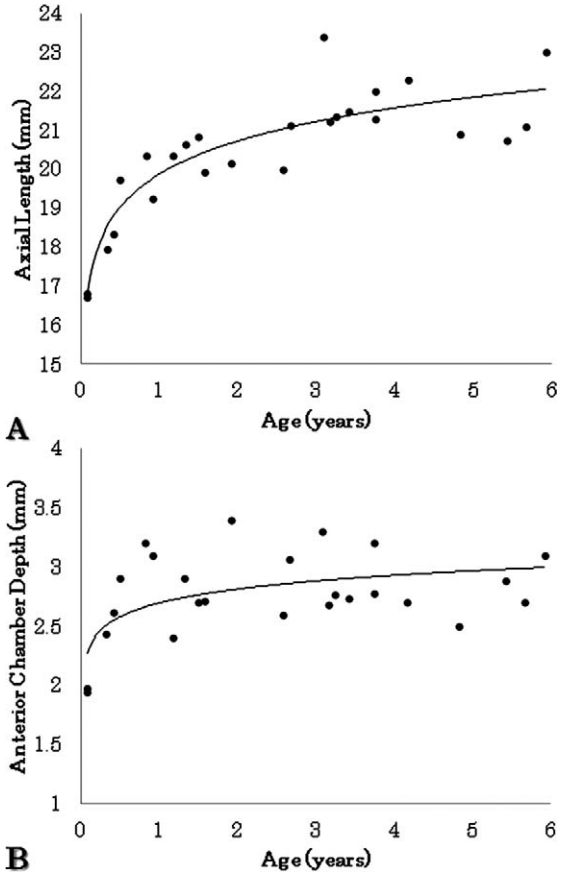

FIGURE 3. Scatterplot of AL, ACD, and age. (**A**, **B**) AL (Pearson's $r = 0.746$, $P < 0.001$) showed a significant correlation with age. Logarithm approximation of AL as a function of age yielded AL = 1.228 × log(Age) + 19.877 ($r = 0.894$). Logarithm approximation of ACD as a function of age yielded ACD = 0.169 × log(Age) + 2.694 ($r = 0.567$).

Statistical Analyses

Measurements of eye dimensions are expressed as means and SD values. Pearson's correlation coefficients determined by bivariate correlation analysis were used to compare factors such as AL, age, spherical equivalent refraction (SER), crystalline lens shape (*D*, *T*, *Ta*, *Tp*, *R*, *Q*), and PCA of EFDs. To investigate the relationships between the crystalline lens shape and axial elongation, AL was defined as a dependent variable, and multiple linear regression analysis was performed with the crystalline lens shape and the principal component of the crystalline lens as independent variables; $P \leq 0.05$ was considered significant. In statistical tests regarding level of significance of independent variables, $t > |2|$ was considered significant. All statistical analyses were performed using commercial statistical software (StatView software version 5.0; SAS Institute, Inc., Cary, NC).

RESULTS

A total of 25 patients (25 eyes; 14 males and 11 females; age, 1 month to 6 years [2.49 ± 1.81 years]) were enrolled in this study. The average AL and ACD of the right eye were 20.44 ± 1.66 mm and 2.78 ± 0.36 mm, respectively. AL was significantly correlated with age (Pearson's $r = 0.746$, $P < 0.001$) and ACD ($r = 0.659$, $P < 0.001$). AL and age were closely correlated by a logarithmic calculation ($r = 0.894$). A scatterplot of AL and age is shown in Figure 3A. ACD and age were closely correlated by a logarithmic calculation ($r = 0.567$). A scatterplot of ACD and age is shown in Figure 3B.

The average SER was 0.24 ± 1.04 D ($n = 22$). SER was significantly correlated with age ($r = -0.435$, $P = 0.042$), and marginally correlated with AL ($r = -0.419$, $P = 0.051$).

The average crystalline lens dimensions (mm) were as follows: *D*, 7.39 ± 1.03; *T*, 3.75 ± 0.41; *Ta*, 1.86 ± 0.19; and *Tp*, 1.94 ± 0.22. The equatorial lens diameter (*D*) was significantly correlated with age ($r = 0.542$, $P = 0.004$), AL ($r = 0.799$, $P < 0.001$), ACD ($r = 0.398$, $P = 0.048$), *T* ($r = 0.401$, $P = 0.046$), anterior *R* ($r = 0.799$, $P < 0.001$), and posterior *R* ($r = -0.739$, $P < 0.001$). *Ta* was significantly correlated with *Tp* ($r = 0.917$, $P < 0.001$), and SER with posterior *R* ($r = 0.445$, $P = 0.037$, $n = 22$). A scatterplot of the crystalline lens dimensions and age is shown in Figure 4.

The average *R* and *Q* values of the anterior lens surface were 6.21 ± 1.74 mm and (4.60×10^{-4}) ± (9.21×10^{-5}), respectively. The average *R* and *Q* values of the posterior lens surface were −4.81 ± 1.07 mm and (2.49×10^{-4}) ± (1.63×10^{-4}), respectively. Therefore, the anterior and posterior lens surfaces within the central 120° zone were almost spherical. The mean RMS errors (mm) of the anterior and posterior fit were (4.68×10^{-5}) ± (4.39×10^{-5}) and (3.62×10^{-5}) ± (2.60×10^{-5}), respectively.

The first principal component (PC1) of the crystalline lens explained 89.15% of the total variance in lens shape, and the PC1 of the eyeball explained 74.23% of the total variance in eyeball shape. The PC1 of the crystalline lens was significantly correlated with age ($r = 0.648$, $P < 0.001$), AL ($r = 0.847$, $P < 0.001$), ACD ($r = 0.649$, $P < 0.001$), *D* ($r = 0.661$, $P < 0.001$), anterior *R* ($r = 0.600$, $P = 0.001$), and posterior *R* ($r = -0.707$, $P < 0.001$). The PC1 of the eyeball was significantly correlated with age ($r = -0.549$, $P = 0.004$), AL ($r = -0.508$, $P = 0.009$), ACD ($r = -0.406$, $P = 0.043$), *D* ($r = -0.510$, $P = 0.008$), and posterior *R* ($r = 0.519$, $P = 0.007$). The PC1 of the crystalline lens was also significantly correlated with the PC1 of the eyeball ($r = -0.469$, $P = 0.001$).

The correlation between the crystalline lens shape and other elements is shown in Table 1. A scatterplot of age and the PC1 of the crystalline lens is shown in Figure 5A. Figure 5B shows the changes in shape variations within the value range of −2SD to 2SD for the PC1 of crystalline lens shape. A model of the average eye calculated on the basis of correlations between age and the principal component of the total variance in shape is shown in Figure 5C. Multiple linear regression analysis revealed a coefficient of determination of 0.754, in

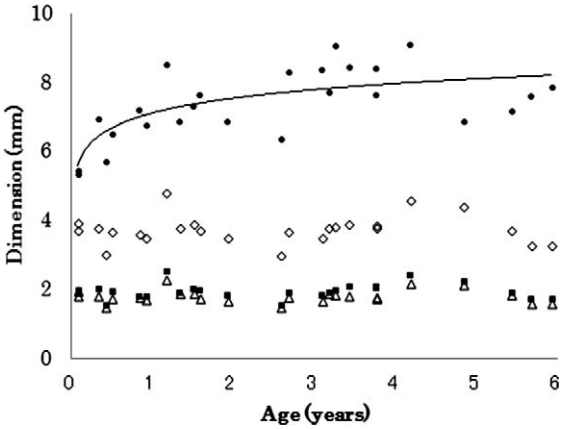

FIGURE 4. Scatterplot of crystalline lens dimensions and age. Age-related changes in *D* (*solid circle*), *T* (*open diamond*), *Ta* (*open triangle*), and *Tp* (*solid square*). Logarithm approximation of *D* as a function of age yielded *D* = 0.613 × log(Age) + 7.104 ($r = 0.718$). Polynomial approximation of *T* as a function of age yielded *T* = −0.0288 × $(\text{Age})^3$ + 0.232 × $(\text{Age})^2$ − 0.444 × (Age) + 3.8653 ($r = 0.347$).

Table 1. Correlation between Crystalline Lens Shape and Other Elements

	Age	Axial Length	ACD	PC1 of Eyeball	SER ($n = 22$)
D	0.542**	0.799***	0.398*	−0.510**	−0.405
T	0.026	0.098	−0.314	−0.113	−0.264
Ta	−0.015	0.032	−0.359	−0.075	−0.267
Tp	0.060	0.150	−0.263	−0.141	−0.251
Anterior *R*	0.439*	0.656***	0.323	−0.311	−0.222
Anterior *Q*	0.271	−0.129	−0.244	−0.015	−0.223
Posterior *R*	−0.651***	−0.755***	−0.417*	0.519**	0.445*
Posterior *Q*	−0.127	−0.325	−0.149	−0.133	−0.267
PC1 of lens	0.648***	0.847***	0.649***	−0.469*	−0.371

Pearson's correlation coefficient: $^{*}P < 0.05$, $^{**}P < 0.01$, $^{***}P < 0.001$.

which AL was a dependent variable. Only the PC1 of the crystalline lens was associated with AL (Table 2). The scatterplots of the anterior and posterior crystalline lens curvatures (*R*) and age, AL, the PC1 of the eyeball, and SER are shown in Figure 6.

Discussion

The results presented here clarify the relationship between changes in the crystalline lens shape and axial elongation in young children. Our results show that the crystalline lens shape changes dramatically during development (Fig. 5). Interestingly, axial elongation was related to the entire contour of the crystalline lens and not to a particular segment (Table 2). These results demonstrate that axial elongation progresses in parallel to change in the crystalline lens shape.

In a previous study, Lotmar[33] reported a Gullstrand model for the eye of newborn infants. That study was based on ocular component dimensions obtained by ultrasonography as well as by the radii of curvature of the crystalline lens measured using deep-frozen sections. The data (mm) were as follows: ACD, 2.54; lens thickness, 3.82; anterior radius, 4.95; posterior radius, 3.66. Recently, Borja et al.[34] reported on the radius of curvature of isolated lens surfaces measured by shadow photography. The calculated anterior and posterior radii of curvature (mm) of newborn infants were 4.46 and 3.47, respectively. On the other hand, Mutti et al.[17] reported clinical data from a large-scale study of newborn infants ($n = 222$) on the basis of dimensions measured by A-scan ultrasonography over the closed eyelid, and keratophakometry measurement of the radius of curvature of the crystalline lens. Data (mm) applying to 3-month-olds were as follows: ACD, 2.76; lens thickness, 3.92; anterior radius, 7.21; posterior radius, 4.68. Both the anterior and posterior radii of curvature measured by Mutti and colleagues were flatter than those obtained by Lotmar[33] and Borja et al.[34] It was believed that these discrepancies originated from the differences in the states of a crystalline lens. According to the Helmholtz theory, the ex vivo crystalline lens is considered to be in a state of maximum accommodation. In contrast, the clinical data from a large-scale study was based on the crystalline lens in a state of cycloplegia.

In our study, all the patients were under sedation and in the tonic accommodation state. Various anesthetic drugs induce myopia in monkeys,[35] which seems to be comparable to tonic accommodation (night myopia) in humans. In a past report, tonic accommodation among 6-year-olds was approximately 2.5 D.[36] Chen et al.[37] reported that tonic accommodation in a neonate was approximately 3 D. Therefore, it was believed that tonic accommodation in children 6 years of age and neonate was almost equivalent. Our mean values for anterior and posterior radii of curvature in children 3 months and older fell in the middle of the range of the data reported by Mutti et al.[17] and Borja et al.[34] (Fig. 6), which was a satisfactory result. However, our data for the crystalline lens of a neonate were similar to those for the isolated lens. It was difficult to determine whether tonic accommodation in the neonate was amplified by triclofos sodium syrup or whether its distribution was individual dependent.

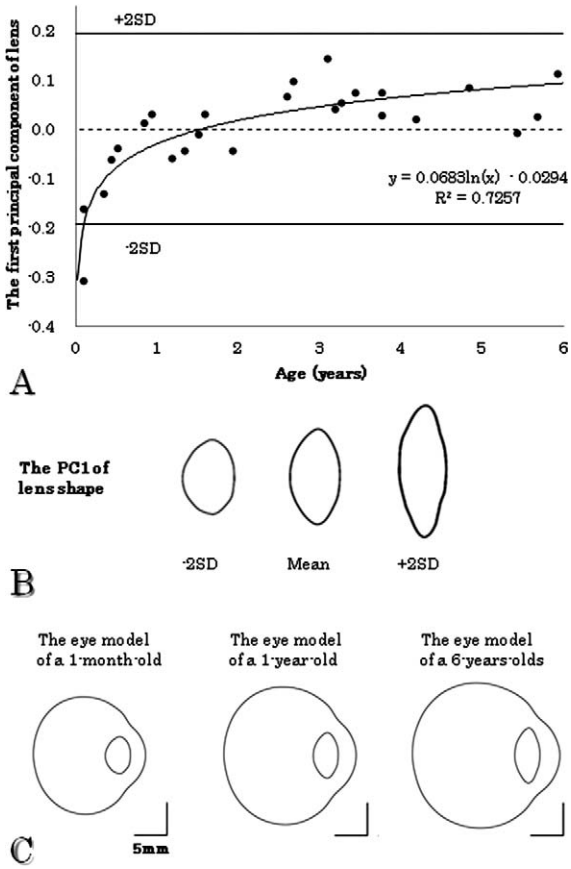

Figure 5. (**A**) Scatterplot of the PC1 of crystalline lens shape and age. The *dotted line* indicates the average value of PC1, and the average value is always set at 0 in the PCA. The *solid line* represents −2SD and 2SD for the PC1. (**B**) Crystalline lens shapes where the PCA by standardized elliptic Fourier descriptors was visualized. Contours drawn in *solid lines* correspond to shapes having the component scores from −2SD to 2SD, respectively. (**C**) The average eye model calculated on the basis of correlations between age and the principal component of the total variance of shape. The average axial length, anterior chamber depth, and lens thickness were allocated for each eye model.

Table 2. Results from Multiple Regression Analysis of Axial Length and Independent Variables in Relation to Crystalline Lens Shape

	β	*t* Value	*P* Value
D	0.160	0.477	0.662
T	−32.833	−0.762	0.458
Ta	15.042	0.749	0.466
Tp	18.657	0.779	0.448
Anterior *R*	−0.279	−0.881	0.392
Anterior *Q*	−0.017	−0.122	0.904
Posterior *R*	−0.500	−1.310	0.210
Posterior *Q*	−0.122	−0.976	0.344
PC1 of lens	0.471	2.548*	0.022†

β, standard regression coefficient.
* Significant at $t > |2|$.
† Significant at $P < 0.05$.

Changes in the anterior and posterior radii of curvature were significantly correlated with axial elongation in our study (Fig. 6). However, such correlations do not confirm that changes in crystalline lens shape and axial elongation are related. It is difficult to establish a reference point for two shapes that change simultaneously. A valid comparison of the changes in the two shapes requires comparison of the entire contour of both shapes. Therefore, we used Fourier transformation of the shape contours. We used the principal component (PC) of elliptic Fourier descriptors (EFDs) to quantitatively evaluate the contour. This value can extract a change in pattern with a large contribution from shape with diversity. Then, the PC can extract the eyeball shape of large contribution from various eyeball shapes, and can evaluate the correlation of two shapes such as the crystalline lens and the eyeball. Moreover, this value can be visually reconstructed as shown in Figure 5B. Our findings revealed that changes in the contours of the crystalline lens (the PC1 of the lens) and the eyeball (PC1 of eyeball) were significantly correlated (Table 1). Multiple linear regression analysis showed that axial elongation was associated with the entire crystalline lens contour, and not a particular segment of the crystalline lens (Table 2). PCA of EFDs is thus a useful tool for shape analyses in ophthalmology.

The equatorial lens diameter (*D*) was significantly correlated with ocular component dimensions, and with the radius of curvature of the crystalline lens. During development, the distance between the crystalline lens and the peripheral sclera (i.e., the length of Zinn's zonule) hardly changed (Fig. 5C). For this reason, it was thought that the extension in the direction of the equator of the crystalline lens originated in peripheral scleral growth. A recent study noted that thinning and flattening of the crystalline lens were necessary for emmetropization.[15] The same study suggested that a mechanical process such as crystalline lens stretching originating in peripheral scleral growth underlies the maintenance of emmetropia. Our results support this hypothesis.

There were some limitations to this study. The possibility of the sample data being biased because the subjects were not prospectively randomly selected was a limitation. Another potential limitation is that because only horizontal images were examined, the overall height of the eyeball was not measured. It is necessary that 1 mm or smaller slice MR images are examined to reconstruct the sagittal image with the horizontal image.[38] In addition, it was difficult to evaluate the reliability and validity of in vivo crystalline lens shape measurement. In a study using 1-mm-slice T2-weighted unprocessed MR images, Jones et al.[39] reported that the porcine lens thickness determined from optical and MR images was almost the same. In our previous study, for a method using 3-mm-slice 3D-reconstructed MR images, the error margin for AL as determined by A-scan ultrasonography and 3D-reconstructed MR image was 0.08 mm. In this study, we used 1.2 to 2.4-mm-

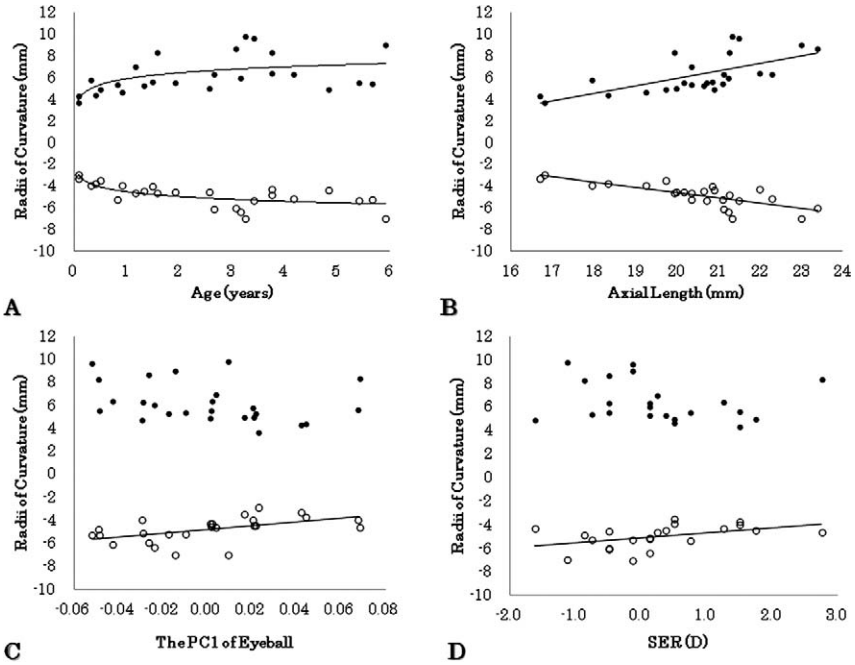

Figure 6. Scatterplots of the anterior (*Ra*; *solid circle*) and posterior (*Rp*; *open circle*) lens radius of curvature and age, AL, PC1 of the eyeball, and SER. (**A**) Logarithm approximation of curvature as a function of age yielded $Ra = 0.791 \times \log(\text{Age}) + 5.846$ ($r = 0.548$) and $Rp = -0.639 \times \log(\text{Age}) - 4.520$ ($r = 0.718$). (**B**) Linear regression of curvature as a function of AL yielded $Ra = 0.688 \times (\text{AL}) - 7.861$ ($r = 0.656$, $P < 0.001$) and $Rp = -0.490 \times (\text{AL}) + 5.193$ ($r = -0.755$, $P < 0.001$). (**C**) Linear regression of curvature as a function of the PC1 of the eyeball yielded $Rp = 16.292 \times$ (PC1 of eyeball) $- 4.814$ ($r = 0.519$, $P = 0.007$). (**D**) Linear regression of curvature as a function of SER: $Rp = 0.421 \times (\text{SER}) - 5.111$ ($r = 0.445$, $P = 0.037$, $n = 22$).

slice 3D-reconstructed MR images. Therefore, moderate reliability of crystalline lens shape measurement was ensured. Although SER was measured during cycloplegia, cycloplegia was not used during MRI. Thus, the correlation coefficient between SER and crystalline lens shape may have been reduced.

In conclusion, we revealed that the crystalline lens shape changes dramatically during development. In addition, axial elongation is related to the entire contour of the crystalline lens, and not to a particular segment. The mechanical stretching in the direction of the equator of the crystalline lens may be a key to resolving emmetropization.

References

1. Wildsoet CF, Howland HC, Falconer S, Dick K. Chromatic aberration and accommodation: their role in emmetropization in the chick. *Vision Res*. 1993;33:1593–1603.
2. Bartmann M, Schaeffel F. A simple mechanism for emmetropization without cues from accommodation or color. *Vision Res*. 1994;34:873–876.
3. Schmid KL, Wildsoet CF. Contrast and spatial-frequency requirements for emmetropization in chicks. *Vision Res*. 1997;37:2011–2021.
4. Schaeffel F, Diether S. The growing eye: an autofocus system that works on very poor images. *Vision Res*. 1999;39:1585–1589.
5. Diether S, Gekeler F, Schaeffel F. Changes in contrast sensitivity induced by defocus and their possible relations to emmetropization in the chicken. *Invest Ophthalmol Vis Sci*. 2001;42:3072–3079.
6. Wildsoet CF, Schmid KL. Emmetropization in chicks uses optical vergence and relative distance cues to decode defocus. *Vision Res*. 2001;41:3197–3204.
7. Wallman J, Turkel J, Trachtman J. Extreme myopia produced by modest change in early visual experience. *Science*. 1978;201:1249–1251.
8. Hodos W, Kuenzel WJ. Retinal image degradation produces ocular enlargement in chicks. *Invest Ophthalmol Vis Sci*. 1984;25:652–659.
9. Mutti DO, Mitchell GL, Jones LA, et al. Accommodation, acuity, and their relationship to emmetropization in infants. *Optom Vis Sci*. 2009;86:666–676.
10. Inagaki Y. The rapid change of corneal curvature in the neonatal period and infancy. *Arch Ophthalmol*. 1986;104:1026–1027.
11. Insler MS, Cooper HD, May SE, Donzis PB. Analysis of corneal thickness and corneal curvature in infants. *CLAO J*. 1987;13:182–184.
12. Mutti DO, Zadnik K, Fusaro RE, Friedman NE, Sholtz RI, Adams AJ. Optical and structural development of the crystalline lens in childhood. *Invest Ophthalmol Vis Sci*. 1998;39:120–133.
13. Wood IC, Mutti DO, Zadnik K. Crystalline lens parameters in infancy. *Ophthalmic Physiol Opt*. 1996;16:310–317.
14. Larsen JS. The sagittal growth of the eye. IV. Ultrasonic measurement of the axial length of the eye from birth to puberty. *Acta Ophthalmol (Copenh)*. 1971;49:873–886.
15. Mutti DO, Mitchell GL, Sinnott LT, et al. CLEERE Study Group. Corneal and crystalline lens dimensions before and after myopia onset. *Optom Vis Sci*. 2012;89:251–262.
16. Twelker JD, Mitchell GL, Messer DH, et al. Children's ocular components and age, gender, and ethnicity. *Optom Vis Sci*. 2009;86:918–935.
17. Mutti DO, Mitchell GL, Jones LA, et al. Axial growth and changes in lenticular and corneal power during emmetropization in infants. *Invest Ophthalmol Vis Sci*. 2005;46:3074–3080.
18. Sorsby A, Sheridan M, Leary GA. Refraction and its components in twins. *M.R.C. Special Report Series, Issue No. 303*. 1962:1–43.
19. van Alphen GW. A correlation matrix of optical elements and age of the human eye. *Exp Eye Res*. 1978;26:573–579.
20. Brown N. The change in lens curvature with age. *Exp Eye Res*. 1974;19:175–183.
21. Cook CA, Koretz JF, Pfahnl A, Hyun J, Kaufman PL. Aging of the human crystalline lens and anterior segment. *Vision Res*. 1994;34:2945–2954.
22. Dubbelman M, Van der Heijde GL, Weeber HA. Change in shape of the aging human crystalline lens with accommodation. *Vision Res*. 2005;45:117–132.
23. Alsbirk PH. Variation and heritability of ocular dimensions. A population study among adult Greenland Eskimos. *Acta Ophthalmol (Copenh)*. 1977;55:443–456.
24. Garner LF, Yap MK. Changes in ocular dimensions and refraction with accommodation. *Ophthalmic Physiol Opt*. 1997;17:12–17.
25. Dubbelman M, van der Heijde GL, Weeber HA. The thickness of the aging human lens obtained from corrected Scheimpflug images. *Optom Vis Sci*. 2001;78:411–416.
26. Strenk SA, Semmlow JL, Strenk LM, Munoz P, Gronlund-Jacob J, DeMarco JK. Age-related changes in human ciliary muscle and lens: a magnetic resonance imaging study. *Invest Ophthalmol Vis Sci*. 1999;40:1162–1169.
27. Strenk SA, Strenk LM, Semmlow JL, DeMarco JK. Magnetic resonance imaging study of the effects of age and accommodation on the human lens cross-sectional area. *Invest Ophthalmol Vis Sci*. 2004;45:539–545.
28. Ishii K, Iwata H, Oshika T. Quantitative evaluation of changes in eyeball shape in emmetropization and myopic changes based on elliptic Fourier descriptors. *Invest Ophthalmol Vis Sci*. 2011;52:8585–8591.
29. Kuhl FP, Giardina CR. Elliptic Fourier features of a closed contour. *Comput Graphics Image Processing*. 1982;18:236–258.
30. Carney LG, Mainstone JC, Henderson BA. Corneal topography and myopia: a cross sectional study. *Invest Ophthalmol Vis Sci*. 1997;38:311–320.
31. Pérez-Escudero A, Dorronsoro C, Marcos S. Correlation between radius and asphericity in surfaces fitted by conics. *J Opt Soc Am A*. 2010;27:1541–1548.
32. Rohlf FJ, Archie JW. A comparison of Fourier methods for the description of wing shape in mosquitoes (*Ritera culicidae*). *Syst Zool*. 1984;33:302–317.
33. Lotmar W. A theoretical model for the eye of new-born infants. *Graefes Arch Clin Exp Ophthalmol*. 1976;198:179–185.
34. Borja D, Manns F, Ho A, et al. Optical power of the isolated human crystalline lens. *Invest Ophthalmol Vis Sci*. 2008;49:2541–2548.
35. Crawford K, Gabelt BT, Kaufman PL, Bito LZ. Effects of various anesthetic and autonomic drugs on refraction in monkeys. *Curr Eye Res*. 1990;9:525–532.
36. Zadnik K, Mutti DO, Kim HS, Jones LA, Qiu PH, Moeschberger ML. Tonic accommodation, age, and refractive error in children. *Invest Ophthalmol Vis Sci*. 1999;40:1050–1060.
37. Chen J, Xie A, Hou L, Su Y, Lu F, Thorn F. Cycloplegic and noncycloplegic refractions of Chinese neonatal infants. *Invest Ophthalmol Vis Sci*. 2011;52:2456–2461.
38. Singh KD, Logan NS, Gilmartin B. Three-dimensional modeling of the human eye based on magnetic resonance imaging. *Invest Ophthalmol Vis Sci*. 2006;47:2272–2279.
39. Jones CE, Pope JM. Measuring optical properties of an eye lens using magnetic resonance imaging. *Magn Reson Imaging*. 2004;22:211–220.